Plasmonic Enhancement of Nanophosphor Upconversion Luminescence in Au Nanohole Arrays

Marjan Saboktakin,[†] Xingchen Ye,[‡] Uday K. Chettiar,[†] Nader Engheta,[†,§,⊥,∥] Christopher B. Murray,[‡,∥] and Cherie R. Kagan[†,‡,∥,*]

[†]Department of Electrical and Systems Engineering, [‡]Department of Chemistry, [§]Department of Bioengineering, [⊥]Department of Physics and Astronomy, and [∥]Department of Materials Science and Engineering, University of Pennsylvania, Philadelphia, Pennsylvania 19104, United States

ABSTRACT Arrays of subwavelength holes (nanoholes) in Au films were computationally designed, fabricated, and used as templates to localize and enhance the luminescence of upconversion nanophosphors (UCNPs)—hexagonal phase $NaYF_4$ doped with Yb^{3+} and Er^{3+}. The dimensions of nanohole Au arrays were designed to accept only a single UCNP upon particle filling and with a periodicity to be resonant with the excitation wavelength of the upconversion. Frequency-dependent luminescence enhancements of up to 35-fold and a concomitant shortening of the UCNP luminescence rise time were observed, consistent with simulations of plasmonic enhancement of the UCNP absorption.

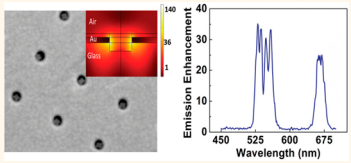

KEYWORDS: upconversion · nanophosphor · nanohole array · plasmonically enhanced luminescence · lanthanide · squeegee method

The desire to control and manipulate light−matter interactions at the nanoscale has become a major scientific interest in recent years as technology shifts progressively toward miniaturization of optical elements and operation with shorter wavelengths of the electromagnetic spectrum. An essential part of nanoscale optical design is the ability to localize electromagnetic fields in dimensions below the diffraction limit and to harvest the resulting enhanced field for which traditionally antennas have been known.[1] Ever since the pioneering report by Ebbesen *et al.*[2] on extraordinary transmission of light through periodic arrays of subwavelength holes in thin metallic films, much effort has been dedicated to exploring the fundamental principles that govern the far-field properties of transmitted light through various types of subwavelength hole arrays as well as the enhancement of the near-field inside each aperture.[3−6] These fundamental studies have yielded many applications of nanohole arrays in areas including efficient chemical and biological sensing[7,8] and enhancement of nonlinear optical effects.[9,10]

A promising application of the high electric field localization in nanoscale structures is to enhance the emission of low quantum yield fluorophors.[11−13] Among such relatively low quantum yield emitters are upconverting nanophosphors (UCNPs) which have attracted much attention in recent years due to their application in various areas including solar cells,[14−17] therapeutics,[18,19] and imaging.[20−22] Among UCNPs, the β-$NaYF_4$ crystal doped with the lanthanide atoms of Yb^{3+} and Er^{3+} remains one of the most efficient upconverting materials.[23] However, it still suffers from relatively low quantum yield.[24] Various nanostructured metallic substrates have been employed for plasmonically enhanced phosphorescence of UCNPs including the use of colloidal nanocrystals,[25,26] arrays of fabricated metallic nanostructures,[27,28] and roughened metallic surfaces.[29,30] The ordered nanohole arrays have a number of advantages: (1) they can be reproducibly fabricated, and their planar geometry promises device scaling and miniaturization; (2) their optical resonances can be systematically tailored through the design of these structures; and (3) each aperture presents a well-defined "template" that could be tailored to host a fixed number of UCNPs with well-defined configurations.

Here, we report dramatic plasmonic enhancement of upconversion luminescence

* Address correspondence to kagan@seas.upenn.edu.

Received for review May 22, 2013 and accepted August 2, 2013.

Published online August 02, 2013
10.1021/nn402598e

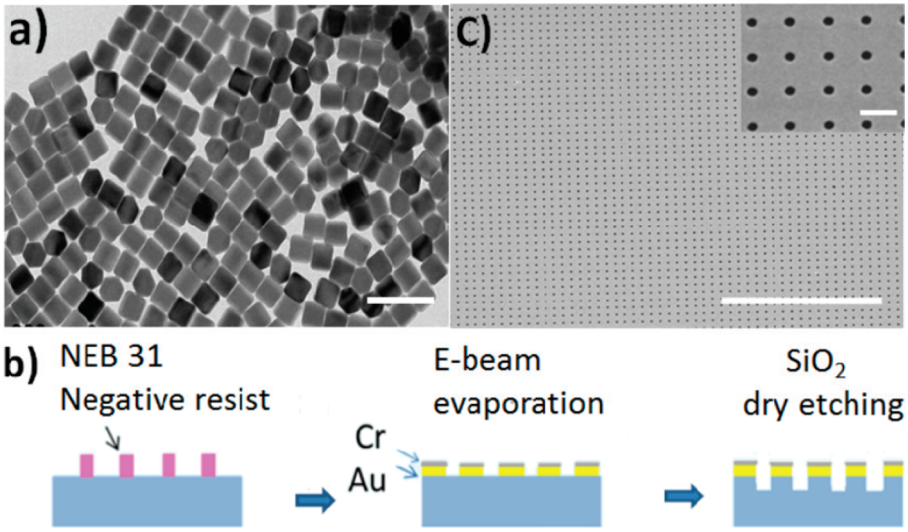

Figure 1. (a) TEM image of hexagonal prismatic $NaYF_4$:Yb^{3+},Er^{3+} UCNPs that are 70 nm in diameter, 80 nm in height. (b) Schematic of the fabrication process used to define Au nanohole arrays. (c) SEM images of the fabricated nanohole arrays at low and (inset) high resolution. Scale bars: (a) 200 nm; (c) main, 10 μm; inset, 500 nm.

in UCNPs by taking advantage of the enhanced electromagnetic field generated in metallic nanohole arrays at resonance. Few works have been devoted to plasmonic enhanced luminescence of molecular dyes and lanthanide atoms using nanohole arrays. In these studies, nanohole arrays in thick (above 100 nm) Au films were fabricated, and the fluorescent molecules or ions were added to the structures through processes such as spin-casting or ion implantation.[31−34] In contrast to previous applications of nanohole arrays, in this work, we design relatively thin metallic layers to minimize the high losses that are often associated with apertures of the commonly used thick metallic layers in nanohole arrays. With this approach, we increased the strength of the electromagnetic field that could be harnessed to enhance the luminescence of UCNPs. To precisely position single UCNPs inside each of the nanohole array apertures, we have employed a "squeegee method".[35] This method allowed precise control over UCNP placement, an essential element in the design and fabrication of next generation devices. We exploited the properties of the nanohole array to create high intensity excitation of the individual UCNPs positioned in each aperture and demonstrated up to 35-fold enhancement in the UCNP luminescence.

The UCNPs used here were Yb^{3+} and Er^{3+} co-doped β-$NaYF_4$ nanocrystals.[36] The UCNPs chosen for filling the nanohole arrays were hexagonal prisms in morphology, having two hexagonal faces with a diameter of ~70 nm and rectangular sides with a height of ~80 nm (standard deviation $\sigma \approx 5\%$). Transmission electron microscopy (TEM) images, represented by Figure 1a, show the UCNPs viewed along various sides of the hexagonal prismatic nanocrystals. Under 980 nm excitation, these UCNPs show a prominent green emission peak at 540 nm and a weaker red emission peak at 650 nm characteristic of sensitization by the Yb^{3+} and upconverted emission from Er^{3+} dopants (Supporting Information Figure S1).[37]

On the basis of the optical absorption and the size of the UCNPs, the nanohole array period and aperture diameters were designed by using COMSOL Multiphysics simulation software and optimized experimentally to give maximum field enhancement inside each aperture and high transmission for the entire array resonant at the 980 nm UCNP excitation wavelength after nanocrystal filling. The resonant wavelength of the metallic nanohole array is dependent on the size of the apertures as well as the periodicity of the array and the thickness of the metallic layer. Given the diameter of the UCNPs, the aperture diameter was made to be 110 nm so that each aperture can host only a single UCNP. In order to minimize losses in the metallic film layer, the thickness of the Au layer was designed to be ~30 nm. Therefore, the period of the array was optimized to be 525 nm.

The Au nanohole arrays were fabricated on transparent glass substrates, in a process depicted in Figure 1b. A negative resist (NEB31a) was patterned using e-beam lithography followed by thermal evaporation of the Au layer. However, since the UCNPs were larger in dimension compared to the thickness of the Au layer and needed to be completely placed inside the aperture to experience maximum field enhancement, the depth of the holes was further increased by dry etching of the glass substrate. Therefore, a thin layer of Cr was evaporated and used as an etch mask to avoid damaging the Au layer during dry etching of the glass substrate. The Au and Cr layers were defined by lift-off of the negative resist. Then, 60 nm of glass was dry etched using CHF_3 chemistry. Nanohole arrays were fabricated across areas of 2 mm × 2 mm. SEM images of a representative Au nanohole array (Figure 1c) show

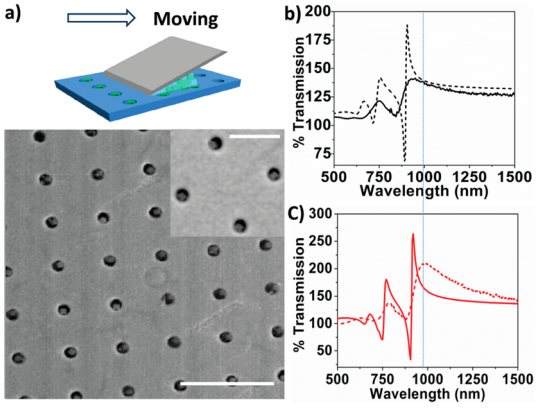

Figure 2. (a) Schematic of the squeegee process used to fill the nanohole array with UCNPs and SEM images of the resulting filled nanohole array. (b) Transmission spectra of the unfilled nanohole arrays based on experimental measurements (solid black) and theoretical simulation results (dashed black) with respect to the transmission from a 30 nm layer of Au deposited on a glass substrate. (c) Transmission spectra of the filled nanohole arrays based on experimental measurements (solid red) and the theoretical simulation results (dashed red) with respect to the transmission from a 30 nm layer of Au deposited on a glass substrate. Scale bars: (a) main, 1 μm; inset, 500 nm.

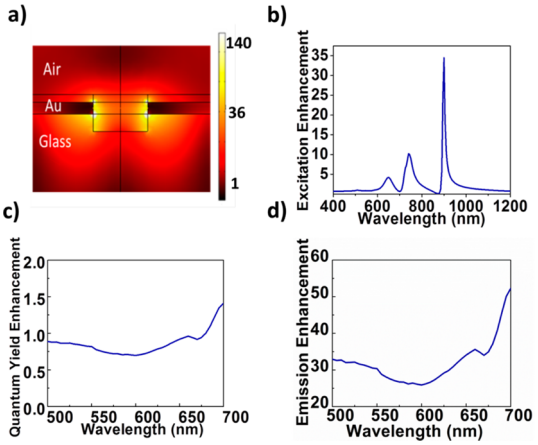

Figure 3. (a) Intensity enhancement inside an aperture in the nanohole array at its resonance normalized with respect to a similar array made in glass. (b) Theoretical simulations for excitation enhancement for the empty nanohole array. (c) Theoretical simulations for quantum yield enhancement of an arbitrary dipole placed in an aperture in the nanohole array at resonance. (d) Theoretical simulations for total emission enhancement of an arbitrary dipole placed in the nanohole array when the pump wavelength is set to the peak of the excitation enhancement.

that precise nanohole arrays were achieved over large areas.

UCNPs were assembled into the Au nanohole arrays by a squeegee process (Figure 2a).[35] A concentrated solution of UCNPs in hexane was placed on the substrate, and a droplet of the UCNP dispersion was slowly swept across the surface of the substrate by a cut piece of polydimethylsiloxane (PDMS). In this method, the meniscus of the droplet which was fixed at the edge of the PDMS piece was dragged across the substrate. As the meniscus moved over holes in the substrate, the UCNPs that were at the meniscus−substrate interface were driven into the holes. By holding the contact angle of the droplet on the substrate at ~35° and using a concentrated UCNP dispersion with a particle concentration of $\sim 1.6 \times 10^{17}$ cm^{-3}, we reproducibly achieved a high filling factor of above 90%. The masking Cr layer was subsequently removed by wet etching, which ensured the removal of any excess UCNPs that remained on the surface of the template during the filling process. Representative SEM images of the resulting filled template are shown in Figure 2a and Supporting Information Figure S2.

Optical transmission measurements were used to characterize the plasmon resonances of empty and UCNP-filled nanohole arrays. The empty nanohole arrays show two major peaks in the transmission spectrum centered at 930 and 780 nm. The transmission peak at 930 nm corresponds to the plasmonic resonance of the entire structure, and the peak at 780 nm arises from diffraction at the metal−glass interface. The broader and less intense resonances measured experimentally in comparison to simulations can be attributed to damping by electron scattering from the Au grains in fabricated structures, which were not taken into account in simulations. The damping effect is notably significant in the small aperture arrays, as the resonant peaks are sharper (Figure 2b). Theoretical simulations and experimental measurements indicated a red shift in the transmission spectrum of the template after filling with UCNPs. The red shift in the spectral features partially arises from the higher refractive index of the UCNPs (~1.4) compared to air in the volumes occupied by UCNPs after particle insertion into each of the apertures (Figure 2c).

It is important to note that the origin of the plasmonic resonance in this nanohole array structure, even though similar in nature, is somewhat different from the arrays that have been used in Ebbessen's report and similar experiments due to the difference in thickness of the metallic layer. In nanohole arrays, where the diameter of the holes is small compared to the thickness of the metallic film, the plasmonic resonance can be best described as excitation of surface plasmon polaritons (SPPs) at the dielectric−metal interface by the incident electromagnetic wave.[5,6] In such structures, the periodic arrays provide the required transverse momentum in order to couple the incident plane wave to the SPP on the surface of the metallic film. However, in the nanohole array structure used here, the diameter of the fabricated apertures is large compared to the thickness of the film. Therefore, the array is instead best described as two intersecting arrays of parallel Au nanostrips that are laid perpendicular to each other forming a fishnet structure. In the presence of an electric field, the nanostrip array perpendicular to the electric field experiences a characteristic plasmonic

resonance at a frequency determined by the geometrical parameters of each strip and the periodicity of the array while the second parallel nanostrip array only acts as a dilute metal simply changing the Drude response of the effective medium by shifting the plasma frequency to lower values.[38−40] Therefore, Ebbesen's approximation and equation for the prediction of transmission peak positions breaks down and is no longer valid in our case. As a result, we have used numerical software to predict the peak positions and field enhancement in the thin metal nanohole array structure used here.

RESULTS AND DISCUSSION

Simulations performed using COMSOL Multiphysics software indicated that, at the resonance of the nanohole array, in the center of each aperture, the electric field is enhanced by a factor of ~6, and therefore, the intensity is enhanced by a factor of ~36 (Figure 3a). The enhancement is greater at hot spots close to the edges of the apertures. The total emission enhancement in fluorophors is the product of both the excitation enhancement and the emitter's quantum yield enhancement. Excitation enhancement refers to the combined effect of the higher absorption rate in Yb^{3+} atoms, as well as the change in the decay rates of the excited states in Yb^{3+} atoms and the intermediate state in Er^{3+} atoms at the pump wavelength. These two effects work together to increase the amount of energy that is transferred to Er^{3+}. Emitter's quantum yield enhancement, however, refers to the change in the decay rates of Er^{3+} atoms at the emission wavelength which would cause an increase in the radiative quantum yield of the emitter atoms.

Since the nanohole array hosting the UCNPs is resonant at the UCNPs' excitation wavelength, we expect that most of the enhancement would arise from the frequency-dependent excitation enhancement. Excitation enhancement simulations revealed up to a 35-fold enhancement at the UCNP absorption. To predict the change in the emitter's quantum yield, simulations were performed for dipoles located at the center of the aperture and averaged over all three directional degrees of freedom (Figure 3c). However, since this effect is strongly distance-dependent, we would expect that for emitters in various locations in an aperture the quantum yield would vary somewhat. The total emission enhancement, calculated as the product of excitation enhancement and emitter's quantum yield enhancement, depicted in Figure 3d, reflects a total enhancement in UCNP emission of ~30 due to the excitation enhancement and changes in dipole quantum yield of the nanophosphors.

Photoluminescence (PL) spectra were collected from $NaYF_4$:Yb^{3+},Er^{3+} UCNPs positioned in the apertures of Au nanohole arrays under 980 nm excitation. A biconvex lens was used to focus collimated 980 nm laser light onto a spot size of ~20 μm in diameter. In order to accurately measure the luminescence enhancement of

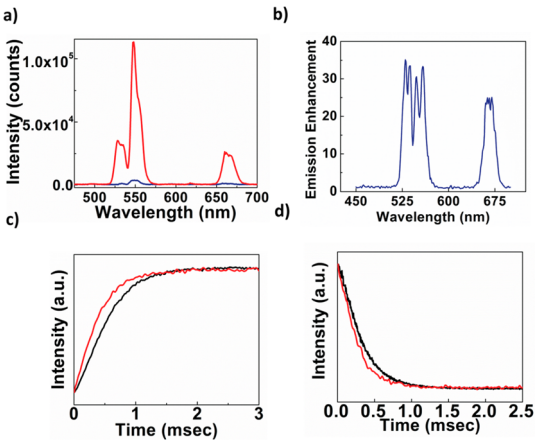

Figure 4. (a) Upconversion luminescence spectra of $NaYF_4$: Yb^{3+},Er^{3+} UCNPs in a glass nanohole array (blue line) and in a Au nanohole array (red line) under 980 nm excitation. (b) Emission enhancement factor as a function of wavelength. Upconversion luminescence (c) rise time and (d) decay time monitoring the 540 nm emission under 980 nm excitation of UCNPs assembled in a glass nanohole array (black line) and in a Au nanohole array (red line).

UCNPs in the Au nanohole array, a similar nanohole array with the same aperture size and periodicity was fabricated in glass. The positive e-beam resist PMMA was patterned by e-beam lithography, and CHF_3 was used to dry etch the SiO_2 substrate, defining the nanohole array. In the glass nanohole array, however, the entire volume of the UCNPs was embedded in the glass templates; therefore, a deeper oxide etching of about 90 nm was performed. The UCNPs were positioned inside the nanohole array with the same squeegee method as described above. After particle filling, the PMMA resist was dissolved using acetone, thereby removing any possible excess particles that had remained on the surface of the resist during the squeegee process (Supporting Information Figure S3). Removal of excess UCNPs ensured that equal numbers of particles were studied in the glass and Au templates, enabling reliable comparison of the emission spectra in the two sample geometries (Supporting Information Figures S2 and S3). The PL spectra for UCNPs localized in both Au and glass nanohole arrays are shown in Figure 4a. We calculated the wavelength-dependent emission enhancement factor by normalizing the emission intensity of the UCNPs in the Au nanohole arrays with respect to that for the same motif of UCNPs in the glass nanohole array (Figure 4b). Enhancements of up to 35-fold were measured near the prominent 540 nm emission peak of the UCNPs. Integration of the area underneath the emission peaks of the UCNPs, averaged over six independent measurements from three samples, showed a 32.6-fold increase for the 540 nm emission peak and a 34.0-fold increase for the 650 nm peak.

Luminescence lifetime measurements performed on UCNPs in the Au nanohole array show a considerable decrease in the rise time of the UCNPs in comparison to the same UCNPs in the glass nanohole array. We

measured a rise time of $\tau = 0.52$ ms for the UCNPs in the nanohole array on glass, while the rise time decreased to $\tau = 0.38$ ms for the case of enhanced UCNPs in the Au nanohole array. This decrease in rise time of UCNPs is consistent with plasmonic enhancement seen in fluorophors, in which the enhancement in excitation intensity accompanies a faster excitation rate in fluorophors.[41]

The quantum yield of UCNPs dramatically influences the magnitudes of the emission enhancement and the lifetime changes they experience in a plasmonic structure. Plasmonic enhancement causes both the radiative and nonradiative rates to increase. In a low quantum yield material, however, the liftetime is dominated by the larger nonradiative rate and does not show the same magnitude of change as the enhancement factor which is largely a measure of the radiative rate.[25]

A decrease in decay time of the UCNPs from 0.3 to 0.25 ms was also measured, which could be attributed to an increase in the radiative rate in those emitter atoms within each UCNP that have an optimum distance between 2 and 10 nm from the Au walls.[25] The increase in radiative rate competes with possible quenching of the emitter, which occurs in very close proximity of less than 2 nm between the emitter and metal layer. However, the quenching effect cannot dominate the process in these particles since only a very small fraction of emitters within individual UCNPs can be in close proximity of the metallic walls to experience quenching. As a result, the dominant effect is the decrease in the decay time of the emitters due to changes in the permittivity of the space surrounding the emitters, which results in an increase in the quantum yield of the emitters.

CONCLUSION

In conclusion, we have designed and fabricated a tunable plasmonic nanohole array resonant at the excitation wavelength of $NaYF_4:Yb^{3+},Er^{3+}$ UCNPs. The array was fabricated by means of reproducible lithographical techniques and was filled by particles using the squeegee method. We further studied the plasmonic emission enhancement of UCNPs placed in these arrays by means of steady-state and time-resolved PL measurements. Luminescence enhancements of up to 35-fold were observed which were due to the combined effects of enhancement in the excitation of sensitizers and increase in radiative decay rate of emitters, which is further supported by the measured decrease in the rise and decay times of the UCNPs in nanohole arrays.

METHODS

Nanocrystal Synthesis. Colloidal UCNPs were synthesized according to our previous work.[36] A typical protocol for the synthesis of hexagonal phase $NaYF_4$-based UCNPs is described below: 5.6 mmol of $NaCF_3COO$ and 3.4 mmol of lanthanide trifluoroacetates together with 15 mL of 1-octadecene (ODE) and 15 mL of oleic acid (OA) were added to a three-necked flask. The mixture was then heated under vacuum at 120 °C for 60 min to form a transparent, yellow solution. The reaction flask was flushed with N_2 for 5 min and was then placed into a molten $NaNO_3/KNO_3$ (1:1 mass ratio) salt bath that was stabilized at 342 °C. A large amount of white smoke was produced after about 1.5 min, indicating the decomposition of metal trifluoroacetates. After 30 min of reaction under N_2 flow and vigorous magnetic stirring, the solution was cooled by adding 15 mL of ODE. The products were isolated by adding ethanol and centrifugation.

Nanohole Array Fabrication. The nanohole arrays were fabricated on Fisher Scientific soda-lime microscope glass. Substrates were first cleaned by sonication in acetone and subsequently by oxygen plasma etching to remove organic residue from the surface. Next, NEB31a negative e-beam resist was spun on the substrates at 4500 rpm followed by 2 min hot plate baking at 110 °C. The patterns were formed by e-beam lithography using an Elionix ELS-7500EX E-beam writer with 20 pA current and 50 kV accelerating voltage. The patterned substrates were subsequently postbaked for 4 min at 90 °C and then developed for 30 s in MF321 developer. Next, a 7 s descumming process was performed on the samples in an Oxford 80+ RIE dry etching tool for 10 s with 30 sccm O_2, 30 mTorr total pressure, and 100 W power. Subsequently, 5 nm Ti adhesion layer, 30 nm of Au, and 15 nm of Cr layer were deposited on the substrate by e-beam evaporation (PVD75 Kurt Lesker). The lift-off process was then performed by soaking the samples in 1165 remover at 70 °C for 30 min followed by a 2 min sonication process. The underlying SiO_2 on patterned samples were subsequently etched ~60 nm in the 80+ RIE dry etching tool using a combination of 12 sccm of Ar and 30 sccm of CHF_3 gases for 80 s. The ~60 nm additional etching into SiO_2 deepened the holes needed for nanophosphor insertion. After the particle filling process, the Cr mask layer was removed by Cr wet etching using standard Cr etchant (Sigma Aldrich) resulting in nanohole arrays with UCNPs filling 90 nm deep apertures.

The nanohole array period and aperture diameters fabricated by e-beam lithography were initially designed by using COMSOL Multiphysics simulation. However, the nanohole array resonance will experience a red shift after the filling process due to the change in the permittivity of the aperture space filled by UCNPs, which is hard to capture in simulations. As a result, several sets of templates were fabricated and their aperture diameter and periodicity were optimized such that the resonance of the filled template would be at the excitation wavelength of UCNPs (980 nm).

Structural and Optical Measurements. Transmission electron microscopy images were taken on a JEM-1400 microscope operating at 120 kV. Scanning electron microscopy was performed on a FEI Quanta 600 ESEM operating at 5 kV. Optical absorption spectra were recorded using a Cary 5000 UV/vis/NIR spectrometer. Upconversion luminescence was measured on a Fluorolog-3 spectrofluorometer (Jobin-Yvon) using excitation from a 980 nm diode laser with 1.06 W power and a 0.05 W/mm^2 power density. A 1 in. diameter biconvex lens with focal length of 25.4 mm was used to focus the light on a ~20 μm spot on the nanohole array patterned area. Photoluminescence lifetime measurements were performed with the same 1 W, continuous wave, 980 nm laser light source. The excitation was modulated at 100 Hz with a Stanford Research Systems SR540 optical chopper, and the time-dependent luminescence was collected using a multichannel analyzer system integrated in the Fluorohub of a Jobin-Yvon Fluorolog-3 spectrofluorometer, which is a time-gated method compatible with the long lifetime of UCNPs.

Simulations. The simulations were performed on a commercial finite element method (FEM) based solver (COMSOL Multiphysics) using a frequency domain solver. The structure was meshed using tetrahedral mesh elements with a resolution

between 2 and 10 nm inside the gold film and a gradually increasing mesh size as we move away from the gold film with a maximum mesh element size of 50 nm. The simulation domain was surrounded by a perfectly matched layer (PML) to absorb the outward propagating radiation. The permittivity of the gold was obtained through ellipsometry measurements on gold films deposited using the same e-beam evaporator that was used in the fabrication of the nanohole array. The total emission enhancement was calculated using the model for upconversion enhancement.[42] The total emission enhancement can be split into two parts, excitation enhancement at the pump wavelength and quantum yield enhancement at the emission wavelength. The excitation enhancement is directly proportional to the fourth power of the local field enhancement by virtue of the upconversion being a two-photon process and inversely proportional to the square of the decay rate of the intermediate level in the upconversion.[42] To calculate the local field enhancement, the structure was illuminated with a plane wave at the pump wavelength and the local field in a hole was simulated. The transmittance spectrum was also obtained using plane wave simulations. The decay rate of the intermediate level was simulated by placing a dipole at the location of the UCNP and calculating the power emitted by the dipole. This power includes both the radiated power and the power absorbed by the plasmonic structure. According to the semiclassical approximation,[43] the ratio of the total power emitted by the dipole is proportional to the total decay rate of a two-level system placed at the same location. The quantum yield enhancements at the emission wavelength were also simulated using the semiclassical approximation,[43] but in this case, we distinguished between the radiated power and the power absorbed by the plasmonic structure. The radiated power is proportional to the radiative decay rate, whereas the absorbed power is proportional to the quenching rate due to the plasmonic structure. By using the intrinsic quantum yield of the UCNP at the emission wavelength, we could calculate the quantum yield in the presence of the plasmonic structure.

Conflict of Interest: The authors declare no competing financial interest.

Acknowledgment. M.S., X.Y., U.C., N.E., C.B.M., and C.R.K. acknowledge support from the Office of Naval Research (ONR) Multidisciplinary University Research Initiative (MURI) on Optical Metamaterials through Award N00014-10-1-0942. C.B.M. is also grateful to the Richard Perry University Professorship for support of his supervisor role.

Supporting Information Available: Luminescence spectra of $NaYF_4$:Yb^{3+},Er^{3+}. Low-magnification SEM image of UCNP-filled Au nanohole array. SEM image of UCNP-filled glass nanohole array after PMMA removal. This material is available free of charge *via* the Internet at http://pubs.acs.org.

REFERENCES AND NOTES

1. Biagioni, P.; Huang, J. S.; Hecht, B. Nanoantennas for Visible and Infrared Radiation. *Rep. Prog. Phys.* **2012**, *75*, 024402.
2. Martín-Moreno, L.; García-Vidal, F. J.; Lezec, H. J.; Pellerin, K. M.; Thio, T.; Pendry, J. B.; Ebbesen, T. W. Theory of Extraordinary Optical Transmission through Subwavelength Hole Arrays. *Phys. Rev. Lett.* **2001**, *86*, 1114–1117.
3. Genet, C.; Ebbesen, T. W. Light in Tiny Holes. *Nature* **2007**, *445*, 39–46.
4. García de Abajo, F. J. Colloquium: Light Scattering by Particle and Hole Arrays. *Rev. Mod. Phys.* **2007**, *79*, 1267–1290.
5. Biswas, R.; Neginhal, S.; Ding, C. G.; Puscasu, I.; Johnson, E. Mechanisms Underlying Extraordinary Transmission Enhancement in Subwavelength Hole Arrays. *J. Opt. Soc. Am. B* **2007**, *24*, 2589–2596.
6. Bonod, N.; Enoch, S.; Li, L.; Evgeny, P.; Neviere, M. Resonant Optical Transmission through Thin Metallic Films with and without Holes. *Opt. Express* **2003**, *11*, 482–490.
7. Sannomiya, T.; Scholder, O.; Jefimovs, K.; Hafner, C.; Dahlin, A. B. Investigation of Plasmon Resonances in Metal Films with Nanohole Arrays for Biosensing Applications. *Small* **2011**, *7*, 1653–1663.
8. Cervantes Tellez, G. A.; Ahmed, A.; Gordon, R. Optimizing the Resolution of Nanohole Arrays in Metal Films for Refractive-Index Sensing. *Appl. Phys. A: Mater. Sci. Process.* **2012**, *109*, 775–780.
9. Airola, M.; Liu, Y.; Blair, S. Second-Harmonic Generation from an Array of Sub-wavelength Metal Apertures. *J. Opt. A: Pure Appl. Opt.* **2005**, *7*, S118–S123.
10. van Nieuwstadt, J.; Sandtke, M.; Harmsen, R.; Segerink, F.; Prangsma, J.; Enoch, S.; Kuipers, L. Strong Modification of the Nonlinear Optical Response of Metallic Subwavelength Hole Arrays. *Phys. Rev. Lett.* **2006**, *97*, 146102.
11. Gerber, S.; Reil, F.; Hohenester, U.; Schlagenhaufen, T.; Krenn, J.; Leitner, A. Tailoring Light Emission Properties of Fluorophores by Coupling to Resonance-Tuned Metallic Nanostrctures. *Phys. Rev. B* **2007**, *75*, 073404.
12. Mahdavi, F.; Liu, Y.; Blair, S. Modeling Fluorescence Enhancement from Metallic Nanocavities. *Plasmonics* **2007**, *2*, 129–141.
13. Lakowicz, J. R.; Ray, K.; Chowdhury, M.; Szmacinski, H.; Fu, Y.; Zhang, J.; Nowaczyk, k. Plasmon-Controlled Fluorescence: A New Paradigm in Fluorescence Spectroscopy. *Analyst* **2008**, *133*, 1308–1346.
14. Briggs, J. A.; Atre, A. C.; Dionne, J. A. Narrow-Bandwidth Solar Upconversion: Case Studies of Existing Systems and Generalized Fundamental Limits. *J. Appl. Phys.* **2013**, *113*, 124509.
15. Ma, X.; Ni, X. Using Upconversion Nanoparticles To Improve Photovoltaic Properties of Poly(3-hexylthiophene)−TiO_2 Heterojunction Solar Cell. *J. Nanopart. Res.* **2013**, *15*, 1547.
16. van der Ende, B. M.; Aarts, L.; Meijerink, A. Lanthanide Ions as Spectral Converters for Solar Cells. *Phys. Chem. Chem. Phys.* **2009**, *11*, 11081–11095.
17. Shalav, A.; Richards, B. S.; Trupke, T.; Krämer, K. W.; Güdel, H. U. Application of $NaYF_4$:Er^{3+} Up-converting Phosphors for Enhanced Near-Infrared Silicon Solar Cell Response. *Appl. Phys. Lett.* **2005**, *86*, 013505.
18. Wang, C.; Cheng, L.; Liu, Z. Drug Delivery with Upconversion Nanoparticles for Multi-functional Targeted Cancer Cell Imaging and Therapy. *Biomaterials* **2011**, *32*, 1110–1120.
19. Chatterjee, D. K.; Gnanasammandhan, M. K.; Zhang, Y. Small Upconverting Fluorescent Nanoparticles for Biomedical Applications. *Small* **2010**, *6*, 2781–2795.
20. Priyam, A.; Idris, N. M.; Zhang, Y. Gold Nanoshell Coated $NaYF_4$ Nanoparticles for Simultaneously Enhanced Upconversion Fluorescence and Darkfield Imaging. *J. Mater. Chem.* **2012**, *22*, 960–965.
21. Jin, J.; Gu, Y.; Man, C. W.; Cheng, J.; Xu, Z.; Zhang, Y. Upconversion Nanoparticles for Charge-Dependent Cellular Imaging. *ACS Nano* **2011**, *5*, 7838–7847.
22. Esipova, T. V.; Ye, X.; Collins, J. E.; Sakadžić, S.; Mandeville, E. T.; Murray, C. B.; Vinogradov, S. A Dendritic Upconverting Nanoparticles Enable *In Vivo* Multiphoton Microscopy with Low-Power Continuous Wave Sources. *Proc. Natl. Acad. Sci. U.S.A.* **2012**, *109*, 20826–20831.
23. Menyuk, N. $NaYF_4$: Yb,Er—An Efficient Upconversion Phosphor. *Appl. Phys. Lett.* **1972**, *21*, 159–161.
24. Boyer, J.-C.; van Veggel, F. C. J. M. Absolute Quantum Yield Measurements of Colloidal NaYF4:Er^{3+},Yb^{3+} Upconverting Nanoparticles. *Nanoscale* **2010**, *2*, 1417–1419.
25. Saboktakin, M.; Ye, X.; Oh, S. J.; Hong, S. H.; Fafarman, A.; Chettiar, U.; Engheta, N.; Murray, C. B.; Kagan, C. R. Metal-Enhanced Upconversion Luminescence Tunable through Metal Nanoparticle−Nanophosphor Seperation. *ACS Nano* **2012**, *6*, 8758–8766.
26. Zhang, H.; Li, Y.; Ivanov, I. A.; Qu, Y.; Huang, Y.; Duan, X. Plasmonic Modulation of the Upconversion Fluorescence in $NaYF_4$:Yb/Tm Hexaplate Nanocrystals Using Gold Nanoparticles or Nanoshells. *Angew. Chem., Int. Ed* **2010**, *49*, 2865–2868.
27. Zhong, L.; Lu, A.; Paudel, H.; Bayat, K.; Baroughi, M.; May, P. S.; Smith, S.; City, R. Spectroscopic Imaging for Characterization of Metal-Enhanced Upconversion. *IEEE Photovoltaic Spec. Conf., 37th* **2011**, *978*, 1758–1761.

28. Zhang, W.; Ding, F.; Chou, S. Y. Large Enhancement of Upconversion Luminescence of $NaYF_4$:Yb^{3+}/Er^{3+} Nanocrystal by 3D Plasmonic Nano-antennas. *Adv. Mater.* **2012**, *24*, 236–241.
29. Aisaka, T.; Fujii, M.; Hayashi, S. Enhancement of Upconversion Luminescence of Er Doped Al_2O_3 Films by Ag Island Films. *Appl. Phys. Lett.* **2008**, *92*, 132105.
30. Managaki, N.; Fujii, M.; Nakamura, T.; Usui, Y.; Hayashi, S. Enhancement of Photoluminescence from Yb and Er Co-doped Al_2O_3 Films by an Asymmetric Metal Cavity. *Appl. Phys. Lett.* **2006**, *88*, 042101.
31. Verhagen, E.; Kuipers, L.; Polman, A. Field Enhancement in Metallic Subwavelength Aperture Arrays Probed by Erbium Upconversion Luminescence. *Opt. Express* **2009**, *17*, 14586–14598.
32. Guo, P.-F.; Wu, S.; Ren, Q.-J.; Lu, J.; Chen, Z.; Xiao, S.-J.; Zhu, Y.-Y. Fluorescence Enhancement by Surface Plasmon Polaritons on Metallic Nanohole Arrays. *J. Phys. Chem. Lett.* **2010**, *1*, 315–318.
33. Brolo, A. G.; Kwok, S. C.; Moffitt, M. G.; Gordon, R.; Riordon, J.; Kavanagh, K. L. Enhanced Fluorescence from Arrays of Nanoholes in a Gold Film. *J. Am. Chem. Soc.* **2005**, *127*, 14936–14941.
34. Liu, Y.; Blair, S. Fluorescence Enhancement from an Array of Subwavelength Metal Apertures. *Opt. Lett.* **2003**, *28*, 507–509.
35. Black, C. T.; Murray, C. B.; Sandstrom, R. L. Embedded Nanoparticle Films and Method for Their Formation in Selective Areas on a Surface. U.S. Patent 7,682,591, 2012.
36. Ye, X.; Collins, J. E.; Kang, Y.; Chen, J.; Chen, D. T. N.; Yodh, A. G.; Murray, C. B. Morphologically Controlled Synthesis of Colloidal Upconversion Nanophosphors and Their Shape-Directed Self-Assembly. *Proc. Natl. Acad. Sci. U.S.A.* **2010**, *107*, 22430–22435.
37. Yi, G. S.; Chow, G. M. Synthesis of Hexagonal-Phase $NaYF_4$:Yb,Er and $NaYF_4$:Yb,Tm Nanocrystals with Efficient Upconversion Fluorescence. *Adv. Funct. Mater.* **2006**, *16*, 2324–2329.
38. Zhang, S.; Fan, W.; Malloy, K. J.; Brueck, S. R. J. Near-Infrared Double Negative Metamaterials. *Opt. Express* **2005**, *13*, 4922–4930.
39. Pendry, J. B.; Martín-Moreno, L.; Garcia-Vidal, F. J. Mimicking Surface Plasmons with Structured Surfaces. *Science* **2004**, *305*, 847–848.
40. Pendry, J.; Holden, A.; Stewart, W.; Youngs, I. Extremely Low Frequency Plasmons in Metallic Mesostructures. *Phys. Rev. Lett.* **1996**, *76*, 4773–4776.
41. Lakowicz, J. R. Radiative Decay Engineering: Biophysical and Biomedical Applications. *Anal. Biochem.* **2001**, *298*, 1–24.
42. Esteban, R.; Laroche, M.; Greffet, J.-J. Influence of Metallic Nanoparticles on Upconversion Processes. *J. Appl. Phys.* **2009**, *105*, 033107.
43. Novotny, L.; Hecht, B. *Principles of Nano-Optics*; Cambridge University Press: New York, 2006.